文章编号：1001－9014(2019)04－0419－07

DOI:10.11972/j.issn.1001－9014.2019.04.005

Simulation of transverse field sweeping system for a MW-class gyrotron with single-stage depressed collector

WANG Kai[1,2], XUE Qian-Zhong[1,2*], ZHANG Shan[1,2], ZHAO Ding[1], ZHANG Lian-Zheng[1]

(1. Key Laboratory of High Power Microwave sources and Technology, Institute of Electronics, Chinese Academy of Sciences, Beijing 100190, China;
2. University of Chinese Academy of Sciences, Beijing 100049, China)

Abstract: The simulation of transverse field sweeping system (TFSS) for a 170 GHz, MW-class gyrotron with single-stage depressed collector (SDC) is presented in this paper. The adoption of SDC aims to recover part residual kinetic energy of spent electrons as well as to improve the total efficiency exceeding 55%. Transverse field sweeping system is coming into use to expand the spent electron trajectory length to 1100 mm to keep the specific heat dissipation on the collector surface within technically acceptable limits. Furthermore the modulation depth of sweeping signal and the number of transverse coils are simulated to get an optimal result 38.9% and 6 leading to an acceptable peak averaged power density 117.1 W/cm^2. In order to ensure the safety and feasibility in actual situation, the cooling system with axial groves for collector is also designed and the thermal and fluid analysis are carried out by commercial available software ANSYS. The maximum temperature of inner and outer collector surface are 156.09 ℃ and 140.35 ℃ respectively. The range of water temperature at the inlet and outlet are 20 ~ 26.68 ℃ and 38.01 ~ 58.56 ℃ respectively.

Key words: gyrotron, single-stage depressed collector, transverse field sweeping system, thermal and fluid analysis
PACS: 84.40.Ik

兆瓦级回旋管单级降压收集极横向磁扫描系统的仿真

王 恺[1,2], 薛谦忠[1,2*], 张 珊[1,2], 赵 鼎[1], 张连正[1]

(1. 中国科学院电子学研究所 高功率微波源与技术重点实验室, 北京 100190;
2. 中国科学院大学, 北京 100049)

摘要：对170 GHz兆瓦级回旋管单级降压收集极横向磁扫描系统进行了仿真. 采用单级降压收集极一方面回收了废电子注的部分活跃能量同时提升总输出效率超过55%. 横向磁扫描系统的引入扩展了废电子注轨迹长度至1100 mm, 使收集极表面热耗散保持在技术允许范围内. 此外仿真得到了扫描信号的调制深度以及横向线圈数的最优结果38.9%和6, 以及可接受的最大平均功率值117.1 W/cm^2. 为了确保在实际工作中的安全性和可行性, 设计了轴向开槽的收集极冷却系统, 利用软件ANSYS开展了收集极的热和流体分析. 得到收集极内外表面的最高温度各自为156.09℃和140.35℃. 进水口和出水口的水温范围分别为20 ~ 26.68℃和38.01 ~ 58.56℃.

关 键 词：回旋管；单级降压收集极；横向磁扫描系统；热和流体分析

中图分类号：TN129　　**文献标识码**：A

Introduction

Gyrotron is a novel high power millimeter-wave and submillimeter-wave device which can generate MW-class long pulse even continuous wave (CW) output power[1-2]. Nowadays, it appears in various applications including material processing, biological imaging, and

收稿日期：2019-01-22，**修回日期**：2019-05-27　　**Received date**: 2019-01-22, **revised date**: 2019-05-27
Foundation items: Supported by National Natural Science Foundation of China (11475182, 61671431)
作者简介(Biography): WANG Kai (1993-), male, Yangquan, China, Ph. D. student. Research fields include high power millimeter source and technology. E-mail: wangkai164@mails.ucas.ac.cn
* **通讯作者(Corresponding author)**: E-mail: qianzhong_xue@mail.ie.ac.cn

plasma heating for the International Thermonuclear Experimental Reactor (ITER) and so on[1-3]. For ITER, the electron cyclotron resonance heating decides the frequency 170 GHz of gyrotron. This program needs 20 MW CW output power in total[4]. So the output power of single gyrotron at 170 GHz must reach at least 1 MW even more. There are many research organizations coming into developing MW-class output power of gyrotron at 170 GHz such as Japanese, Russian and European groups[5-6].

The collector is a critical component of a gyrotron which would dissipate the residual power of spent electrons after interaction with RF field in cavity. High power density tends to melt the collector wall resulting in reducing degree of vacuum in whole tube. Simultaneously, during the operation of long pulse even continuous wave (CW), the high power loading may give rise to metal fatigue in inner collector wall easily. The typical efficiency of a gyrotron is 30% ~35%[7-8]. Since the output power of a gyrotron at 170 GHz needs to reach 1 MW at least, the residual power is still in MW-class level with calculating efficiency above. So it's significant to reduce dissipated power density to an accept level usually 500 W/cm^2 for OFHC or 1 000 W/cm^2 for Glidcop[9].

The power density is associated with total power as well as deposition area and in direct proportion to power, area reversely. Thus, there are two ways to achieve above goal. One is reducing total power namely using depressed collector where the potential of collector is lower than body potential to generate a decelerating electrostatic field recovering electron energy longitudinally. Besides, it's meaningful to require high efficiency for high power gyrotron, the use of depressed collector can also enhance the total efficiency above 50% by recovering part kinetic energy of spent electrons. The other is increasing total electron spreading areas namely using magnetic sweeping system including transverse field sweeping system (TFSS) and vertical field sweeping system (VFSS). The VFSS always shows upper and lower turning points with nearly equal maximum peak power density. The coil frequency is limited to 5 ~ 10 Hz due to eddy current excited by high coil frequency weakening the magnetic field penetrating. Then advanced transverse field sweeping system (TFSS) catches our eyes[10-11]. The sweeping frequency of TFSS is up to 50 Hz which is much higher than VFSS's. The power supply for TFSS is 3-phase AC thyristor controller which is much simpler and cheaper than VFSS's. Above two merits make TFSS have more promising prospect[12].

In this paper, Sect. 1 presents the analysis of single-stage depressed collector. The depressed potential 30 kV and the calculated total efficiency exceeding 55% have been achieved. Section 2 presents the concept of TFSS, then analyzes the effect of the number of TF_coils and modulation depth of sweeping signal on peak averaged power density. Section 3 gives the thermal and fluid analysis by finite element software ANSYS.

1 Single-stage depressed collector analysis

A collector is one of most important component of gyrotron. As axial magnetic field reducing, the gyration radius of electron is increasing and transverse energy convert into axial kinetic energy dissipated in collector wall with heat. Because only transverse energy of electron beam can interact with RF field and the interaction efficiency is relatively low, plenty of electron energy have no contribution to RF output power and are wasted in vain. This behavior limits the whole efficiency of high power gyrotron as well as the power capacity of collector. The depressed collector is capable of recovering axial electron energy with retarding electrostatic field produced by potential difference between collector and body of tube. For the sake of easy fabrication and cost effectiveness, we adopt single-stage depressed collector here.

The operating parameters of electron beam are V_{beam} =80 kV, I_{beam} =70 A, pitch factor α =1.3, an average guiding center radius of 10.1 mm in cavity. The 35% electronic efficiency has been used to calculate the beam power after interaction with RF for a gyrotron at a frequency of 170 GHz and the residual beam power is approximately 3.64 MW. The energy distribution of spent electron is obtained by beam-wave interaction code. The choice of reasonable decelerating potential need to avoid reflected electrons and recover residual energy as more as possible.

The collector is electrically isolated from body of tube with a high voltage ceramic insulator. The decelerating potential is 30 kV, the maximum electric field strength is supposed to satisfy vacuum constraint which the breakdown strength is 10 kV/mm, otherwise the unwished pulse shortening and damaged surface may appear. The depressed collector has been simulated and optimized by using CST Particle Studio software. The optimal collector radius and thickness are 400 mm and 3 mm, respectively. Figure 1 shows the equipotential lines and electron trajectory on collector. The maximum electric field strength is 1.12 kV/mm which is low enough to achieve the vacuum condition. The collector efficiency η_c and the total efficiency η are calculated by

$$\eta_c = \frac{P_c}{(1-\eta_e)P_{\text{beam}}}, \quad (1)$$

$$\eta = \frac{\eta_e}{1-(1-\eta_e)\eta_c}, \quad (2)$$

where P_{beam} is total beam power, η_e is electronic efficiency equally the ratio of RF output power to total beam power and P_c is recovered power. The calculated collector efficiency is 57% with η_e 35% . Simultaneously, the total efficiency η exceeding 55% has been achieved. The dissipated power density distribution is showed in Fig. 2. Figure 2 indicates that the spent electrons impinge inner collector wall with a deposited area nearly 450 mm. The maximum power density is about 482 W/cm^2 within the limit condition 500 W/cm^2 for OFHC copper. But the power density distribution is inhomogeneous and the maximum power density is still in a high level remaining a small safety margin, resulting in a higher requirement for the design of collector cooling system. So we employ the magnetic field sweeping system for collector in order to smoothen power density distribution as well as to reduce power density further.

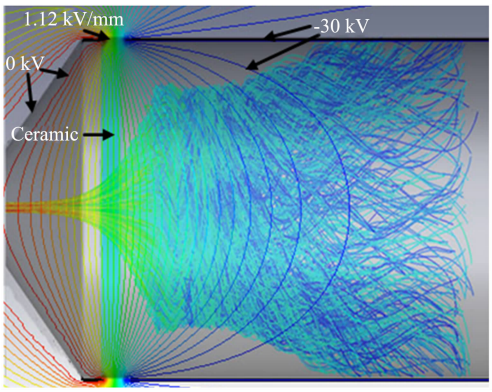

Fig. 1　The equipotential lines and electron trajectory
图 1　等电势线和电子轨迹图

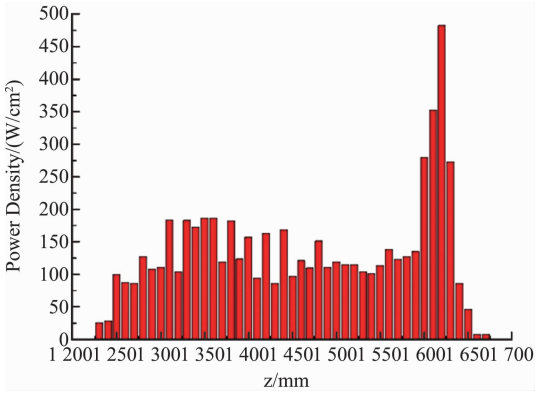

Fig. 2　The dissipated power density distribution along z axis
图 2　沿 z 轴耗散功率密度分布图

2　Simulation and analysis of TFSS

The TFSS usually consists of two or three pairs of solenoid coils called TF_coils which are generating transverse sweeping magnetic field and one solenoid coil called VF_coil which is generating static longitudinal magnetic field. The former is powered by AC power supply while the latter is powered by direct current power supply. Here we employ three pairs of coils namely 6 coils which have 60 degrees phase shift between two adjacent coils. That is to say the phase constant equals 0°, 60°, 120°, 180°, 240°, 300° for each coil respectively[10]. Six TF_coils generate rotating magnetic field which would cause elliptic shape of electron trajectory rather than circle as usual. This behavior spreads out electron deposition area and increases trace length so that lowering the peak power density obviously. The Fig. 3 show elliptic electron trajectory clearly from different views.

To find out the influence of number of TF_coils on dissipated power density, we keep it constant that the size and radial height of TF_coil to see variation of the peak power density and spread trace length by changing coil numbers. The simulated results are listed in table 1.

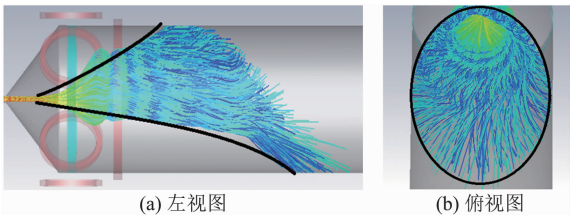

(a) 左视图　　(b) 俯视图

Fig. 3　The elliptic electron trajectory
图 3　椭圆电子轨迹

Table 1　The simulated results with variation of TF_coil number
表 1　横向场线圈数变化结果

Number of TF_coil	4	5	6	7
Peak power density/W/cm^2	243.68	138.57	128.73	121.56
Trace length /mm	850	930	1040	1340
Azimuthal distance /mm	722.57	578.05	481.71	412.90

From Table 1, it is seen that azimuthal distance between adjacent coils decrease with the number of TF_coil increasing, the trace length of spent electron increase and peak power density on collector surface decrease. When the number of TF_coil increases from 6 to 7, the peak power density reduces by approximately 7 W/cm^2, while the trace length of dissipated electrons increases by nearly 300 mm, which means the influence on peak power density generated by number of TF_coil has become weaker and weaker and results in larger collector longitudinal size. Besides, thinking the condition of current power supply for solenoid coil, it's feasible to choose 3 pairs of coils namely 6 coils as transverse field sweeping system.

Other parameters of TFSS geometry are listed in Table 2. The whole profile of TFSS is showed in Fig. 4.

Table 2　The parameters of TFSS geometry
表 2　TFSS 结构参数

	Radial height /mm	Axial height /mm	Supplied current/ (kA-turns)
TF_coil	460	700	18
VF_coil	427	930	13.5

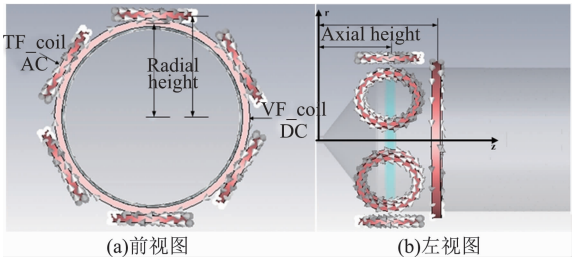

(a)前视图　　(b)左视图

Fig. 4　The whole profile of TFSS
图 4　TFSS 结构图

The dissipated power density distribution is vital to next thermal analysis and its peak value determines maximum hot temperature of collector surface. Since the supplied current wave varies cyclically in time, the time-av-

eraged power density has been employed to measure dissipated power density distribution.

To calculate time-averaged power density, the instantaneous power density and their corresponding weights in time must be gotten first, then multiplying them and getting a sum at different time. As for sweeping signal which is saw tooth or triangular wave, the weights are equal in any time. But sinusoidal signal has a various rates of descent or climbing corresponding to different weights. The variation between rates and weights are in opposite direction which means that high rates represent low weights and low rates represent high weights. Besides the value of weights are related to samples that we take in current cycle.

The profile of peak power density with different samples is showed in Fig. 5. When samples are close to $36 \times 2^9 = 18\,432$, the peak power density reaches to a nearly constant 128.7 W/cm^2 with an increasing percentage of 0.12% only. For samples we take above, the single integral interval is small enough namely 0.02° for one cycle 360° as showed in Fig. 6. And the whole dissipated power density distribution on collector wall with peak power density 128.7 W/cm^2 is showed in Fig. 7.

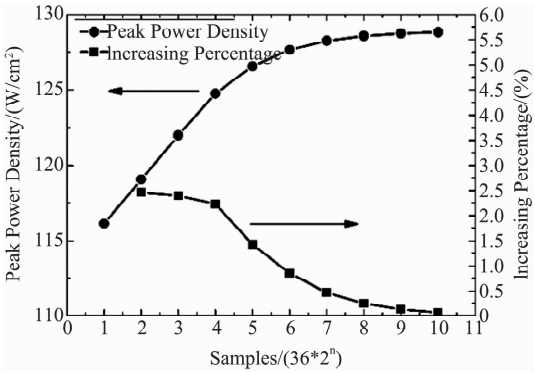

Fig. 5 The profile of peak power density with different samples

图5 不同采样点下最大功率密度曲线

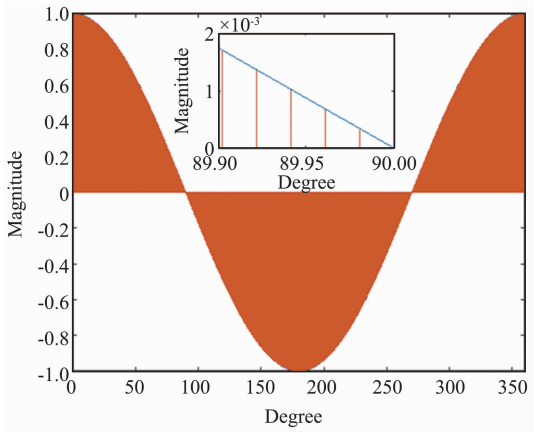

Fig. 6 The divided intervals for one current cycle

图6 一个电流周期下的区间分割图

It's inevitable to give rise to some unexpected errors in practical fabrication process due to misalignments and

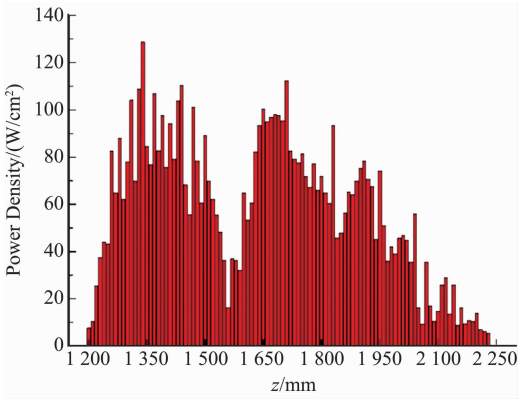

Fig. 7 The whole dissipated power density distribution on collector wall with peak power density 128.7 W/cm^2

图7 最大功率密度 128.7 W/cm^2 对应的收集极壁耗散功率密度分布图

machining errors. The sensitivity analysis have been performed about the effect of the location of TFSS on peak power density. The simulated results are illustrated in Fig. 8. Figure 8 (a) shows the variation of peak power density as a function of axial deviation. The peak power density are fluctuated in a range from 127 W/cm^2 to 134 W/cm^2 with a maximum deviation of 4.1%. As showed in Fig. 8 (b), the peak power density increases relatively quickly when radial deviation becomes larger than 3 mm. But the peak power density is no more than 135 W/cm^2 with a maximum deviation less than 5%.

In order to reduce peak power density further, a way of modulated transversal sweeping has been adopted. The lower peak power density alleviates the limited conditions of the design about water cooling system of collector, supports the stable and long time operation of gyrotron.

For modulated transversal sweeping, it's a varied value in time that not only magnitude but also phase of coil current. In that case, the electron trajectory has a sweeping rotating motion on collector inner wall and moves back and forth along the symmetric z axis at the same time. The local hot spots will be shifted up and down scattering to ambient area so that the peak power density is going be reduced obviously.

We utilize the modulated signal waveform of sinusoid. The optimal modulated frequency 10 Hz has been employed to simulate the influence of modulation depth between the average and the max range of current magnitude on peak power density. The simulation result is showed in Fig. 9. The larger modulation depth may result in higher peak power density due to reducing electrons strike areas. Finally the optimal modulation depth of 38.9% has been found with a peak power density only 117.1 W/cm^2 and the power density distribution is showed in Fig. 10. This behavior enhances the collector power density capacity by a factor of 1.09 and 1.76 compared to unmodulated transversal sweeping and SDC without TFSS leading to a higher safety margin for collector of gyrotron.

The table 3 gives a comparison between this schemes and other existing schemes from several aspects

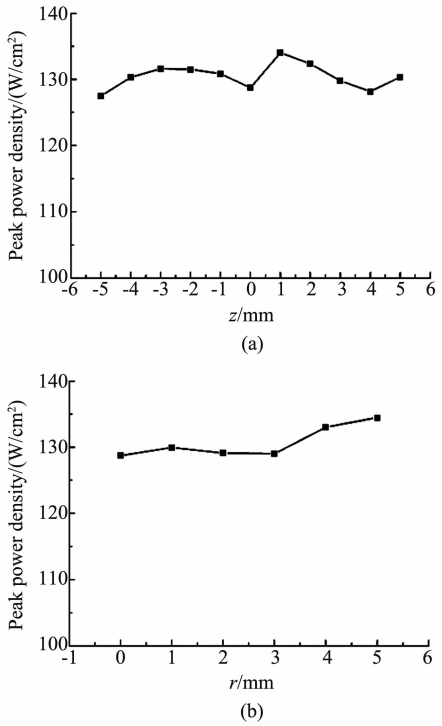

Fig. 8　(a) The peak power density as a function of axial deviation, and (b) radial deviation
图 8　(a)轴向偏移引起的最大功率密度变化,(b)径向偏移引起的最大功率密度变化

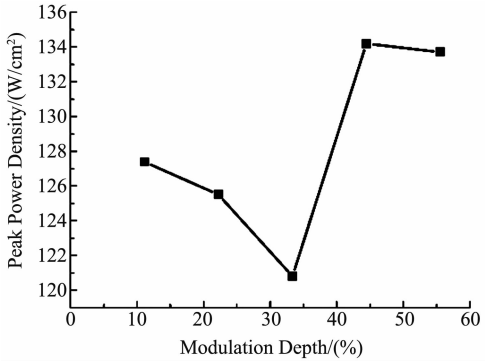

Fig. 9　The peak power density of different modulation depths
图 9　不同调制深度下最大功率密度变化

including operating frequency, collector dissipated power, adopted schemes and peak power density[13-14]. The schemes 1 operates in lower values both in operating frequency and collector dissipated power. The peak power density is 130 W/cm^2 with TFSS only. The schemes 2 employs VFSS with peak power density above 400 W/cm^2. Furthermore, the power supply for VFSS is much more complex and expensive than TFSS's. This schemes adopt the same techniques with the schemes 3. Nevertheless, the collector dissipated power and peak power density are nearly twice and quarter respectively compared to schemes 3. The lower power density guarantees higher operating safety margin as well as enhances power capacity of collector to a large extent. At the same time, it also offers the possibility of higher RF power output for single gyrotron at 170 GHz.

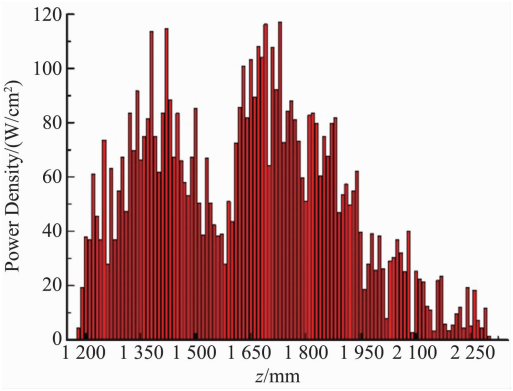

Fig. 10　The power density distribution with modulation depth of 38.9%
图 10　调制深度 38.9% 对应的功率密度分布

Table 3　The comparison between this schemes and other existing schemes
表 3　本文和其他现有方案的比较

	Operating frequency/GHz	Collector dissipated power/MW	Adopted schemes	Peak power density /(W/cm^2)
Schemes 1	94	0.1	TFSS	130
Schemes 2	170	4.2	VFSS	430
Schemes 3	170	1.5	TFSS, Modulation	435
This schemes	170	3.6	TFSS, Modulation	117

3　Thermal and fluid analysis

The thermal analysis of collector is necessary to ensure the safety and feasibility in actual situation. The enormous heat generated by dissipated power transfer from inner surface to outer surface of collector wall by conduction and then are absorbed by coolant due to convection motion. The influence of heat radiation is neglected in this case. The oxygen free high conductivity (OFHC) copper is used as collector material and deionized water is used as coolant. The non-uniform power density distribution are loaded on inner collector wall as heat flux in commercial available software ANSYS for more accurate simulations.

The design of collector cooling system with axial grooves has been taken into account which has a capability of reducing the temperature of collector wall at some extent for more interface with coolant compared to the surface without grooves. The single groove geometry is showed in Fig. 11. The parameters of groove geometry are groove width 5°, groove height 5 mm, groove number 45, the corresponding hydraulic diameter is 8.8 mm. Furthermore, the water flow rate is 900 L/min, the initial water temperature is 20℃. The contour plot of temperature distribution on collector with/without TFSS are showed in Fig. 12(a-b). A comparison is summarized in Table 4. The maximum temperature of collector inner or outer surface without TFSS exceed two times higher than those with TFSS, as well as the constrained temperature

300℃ for collector material.

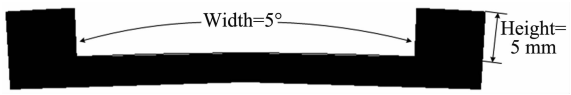

Fig. 11 The structure of single groove
图 11 单槽结构

Table 4 The temperature distribution on collector with TFSS and without TFSS
表 4 采用与不采用 TFSS 造成的收集极温度分布

	Power density/ (W/cm^2)	Collector inner surface/℃	Collector outer surface/℃
With TFSS	117.1_{max}	173.27_{max}	159.02_{max}
Without TFSS	482_{max}	452.27_{max}	406.59_{max}

This high temperature value gives a serious result which plenty of copper molecule have been evapotranspired to high voltage ceramic insulator. So the insulating property has been deteriorated between collector and body of tube leading to a bad performance for gyrotron. This comparison implies that the implement of TFSS is indispensable to make sure high effective and stable operation of tube. It is also showed in Fig. 13 that the profile of temperature distribution of collector inner wall along z axis corresponding to Fig. 12 (a). The profile has a great agreement with dissipated power density distribution in Fig. 10. There are two peak values positioned in approximately 200 mm and 500 mm from original point.

Besides the effect of water flow rate is also studied with identical groove geometry above. The result is obtained in Fig. 14 and corresponding simulated calculating results for heat transfer coefficient and Reynolds number are showed in Fig. 15.

With the increase of water flow rate, the maximum temperature of inner or outer collector wall reduce gradually whereas the heat transfer coefficient and Reynolds number increase. And when water flow rate becomes higher than 600 L/min, the declining rate of maximum temperature becomes lower and lower. The heat transfer coefficient alpha α and Reynolds number Re are determined by following two equations:

$$\alpha = B\frac{v^{0.8}}{D_e^{0.2}} \quad , \quad (3)$$

where B is a constant determined by the physical characteristics of coolant. , v is the velocity of water and the D_e is the hydraulic diameter[15]. Since the geometry of groove remains constant, the hydraulic diameter has no change and alpha will increase with the increase of water flow rate. The heat transfer coefficient α characterizes the capability of transferring heat from solid to fluid. Thus the higher alpha means more heat in collector wall will be absorbed by the coolant deionized water and of course the maximum temperature of inner or outer collector surface become lower.

$$R_e = \frac{v \cdot D_e}{\nu} \quad , \quad (4)$$

where ν is the kinematic viscosity of the fluid[16]. As the geometry of groove and the characteristics of coolant remain constant, the D_e and ν have no change. So the Reynolds number R_e is in direct proportion to the water flow rate. Finally, we take water flow rate 1 100 L/min namely the water velocity 2.3 m/s for each groove as the optimal value within the experimental tolerance limit[15,17]. In this case, the alpha is 6 000 $W/m^2 \cdot ℃$ and the R_e is 20062 which means the coolant DI water is turbulent flow so the capability of transferring heat is in the highest level among three kinds of liquid conditions, laminar, transient and turbulent. The temperature distribution of collector cooling system is listed in Table 5. The maximum temperature of collector surface and outer water are lower than safety limit 300℃ and 70℃, respectively.

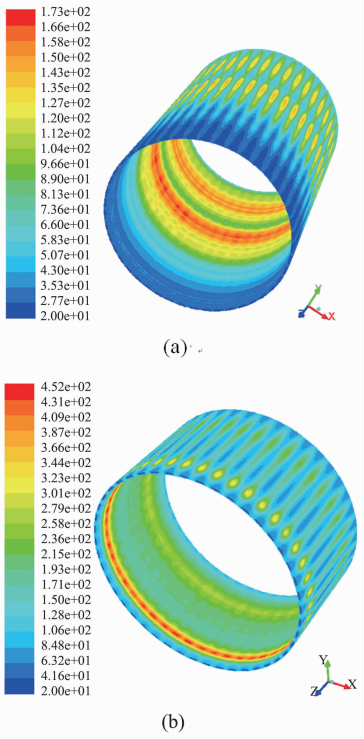

Fig. 12 The contour plot of temperature distribution on collector (a) with TFSS, (b) without TFSS
图 12 收集极温度分布云图 (a)采用 TFSS,(b)不采用 TFSS

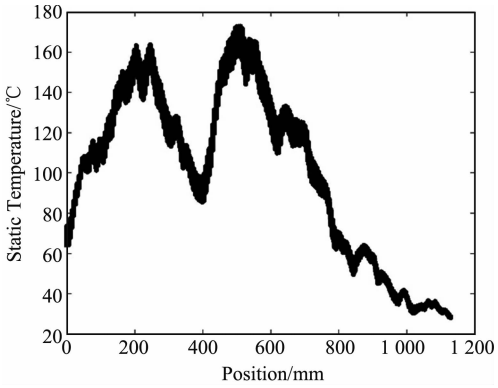

Fig. 13 The profile of temperature distribution of collector inner wall along z axis
图 13 收集极内壁沿 z 轴温度分布

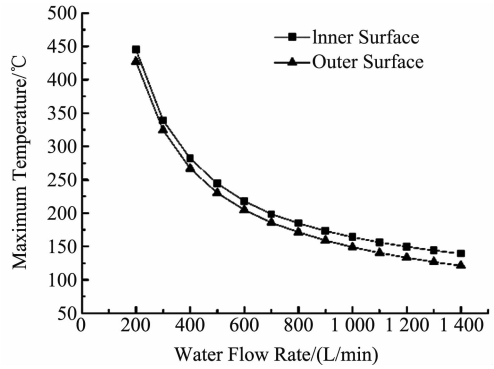

Fig. 14　The effect of water flow rate
图 14　水流速度的影响

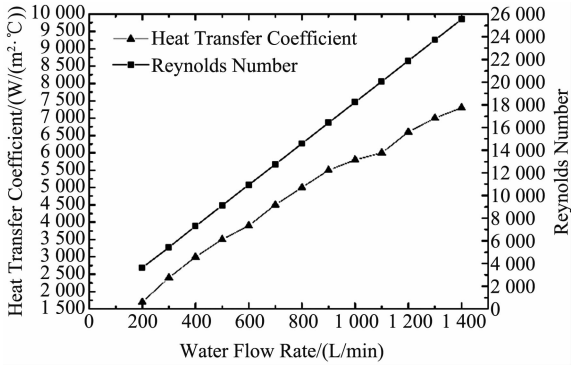

Fig. 15　The variation of heat transfer coefficient and Reynolds number about water flow rate
图 15　水流速度引起的换热系数和雷诺系数变化

Table 5　The temperature distribution of collector cooling system
表 5　收集极冷却系统的温度分布

	Collector inner surface	Collector Outer surface	Inlet water	Outlet water
Temperature/℃	156.09_{max}	140.35_{max}	20 ~ 26.68	38 ~ 58.56

4　Conclusion

The single-stage depressed collector enhances the total efficiency of tube exceeding 55%. The transverse field sweeping system spreads out spent electron trajectory length from 450 mm to 1 100 mm. Thus, the peak power density reduces to 128.7 W/cm^2 from 482 W/cm^2. As the supplied current of TFSS was modulated by 10 Hz sinusoid wave, the peak power density reduces to 117.1 W/cm^2 with the modulation depth of 38.9% further. The number of TF_coils has been chosen to 6 according to peak power density and the feasibility of power supply. The thermal and fluid analysis are carried out by ANSYS code. The simulated results show that the maximum temperature of inner and outer collector wall are 156.09℃ and 140.35℃ respectively with groove number 45, groove width 3°, water flow rate 1 100 L/min. The implementation of SDC and TFSS confirm the increase of total efficiency and the reduction of power density. These results bring specific guidance for the development of a MW-class gyrotron.

Acknowledgement

This work was supported by National Natural Science Foundation of China under Grant No. 11475182 and 61671431. The authors want to thank all team members in our laboratory for their continuous support and encouragement.

References

[1] Felch K L, Danly B, Jory H R, *et al*. Characteristics and applications of fast-wave gyrodevices [J]. *Proceedings of the IEEE*, 1999, **87**(5): 752 - 781.
[2] Flyagin V A, Gaponove A V, Petelin I, *et al*. The gyrotron [J]. *IEEE Transactions on Microwave Theory and Techniques*, 1977, **25**(6): 514 - 521.
[3] Thumm M. Novel applications of millimeter and submillimeter wave gyro-devices [J]. *International Journal of Infrared Millimeter Waves*, 2001, **22**(3): 377 - 386.
[4] Henderson M A, Alberti S, Benin P, *et al*. EU developments of the ITER ECRH system [J]. *Fusion Engineering and Design*, 2007, **82**(5-14): 454 - 462.
[5] Litvak A, Sakamoto K, Thumm M. Innovation on high-power long-pulse gyrotrons [J]. *Plasma Physics and Controlled Fusion*, 2011, **53**(12): 124002.
[6] Thumm M. State-of-the-art of high power gyro-devices and free electron masers update 2003, scientific report FZKA6957 [R]. Forschungszentrum Karlsruhe, Germany, 2004.
[7] Khatun H, Bhattacharya R, Sharan S, *et al*. Design of single-stage depressed collector for 42 GHz, 200 kW gyrotron [J]. *Vacuum*, 2012, **86**(10): 1465 - 1469.
[8] Thumm M. State-of-the-art of high power gyro-devices and free electron masers update 2013, scientific report FZKA7662 [R]. Forschungszentrum Karlsruhe, Germany, 2014.
[9] Schmid M, Illy S, Dammertz G, *et al*. Transverse field collector sweep system for high power CW gyrotrons [J]. *Fusion Engineering and Design*, 2007, **82**(5-14): 744 - 750.
[10] Manuilov V N, Smirnov D A, Malygin S A, *et al*. Numerical simulation of the gyrotron collector systems with rotating magnetic field [C]. *International Conference on Conference Digest of the Joint International Conference on Infrared & Millimeter Waves*, Germany: IEEE, 2004. 663 - 664.
[11] Dammertz G, Illy S, Piosczyk B, *et al*. Collector sweeping systems for high power gyrotrons [C]. *Joint International Conference on Infrared & Millimeter Waves & International Conference on Terahertz Electronics*, USA: IEEE, 2005. 293 - 294.
[12] Braune H, Erckmann V, Illy S, *et al*. Transverse field collector sweeping for the W7-X gyrotrons-modulation techniques [C]. *International Conference on Infrared*, south Korea: IEEE, 2009.
[13] Wang Y R, Geng Z H, Wang H S, *et al*. Simulation of transverse field sweeping system and thermal analysis of an undepressed collector for a gyrotron [J]. *Jouranl of Electromagnetic Waves and Applications*, 2017: 1 - 10.
[14] Illy S, Kern S, Pagonakis I G, *et al*. Collector loading of the 2 MW, 170 GHz gyrotron for ITER in case of beam power modulation [J]. *IEEE Transactions on Plasma Science*, 2013, **41**(10): 2742 - 2747.
[15] Ding Y G. *Design, manufacture and application of high power klystron* [M]. Beijing: National Defense Industry Press, 2010.
[16] Kumar A, Goswami UK, Poonia S, *et al*. Integrated design of undepressed collector for low power gyrotron [J]. *Journal of Infrared Millimeter & Terahertz Waves*, 2011, **32**(6): 733 - 741.
[17] Baxi C B, Callis R W, Gorelov I A, *et al*. Thermal stress analysis of 1 MW gyrotron collector [J]. *Fusion Engineering and Design*, 2007, **82**(5-14): 731 - 735.